*M*1-*E*2 interference in the Zeeman spectra of Bi I

S. Werbowy and J. Kwela*

Institute of Experimental Physics, University of Gdańsk, Wita Stwosza 57, 80-952 Gdańsk, Poland

Studies of the *M*1-*E*2 interference effect in the mixed-type forbidden lines 461.5, 647.6, and 875.5 nm of Bi I are reported. A special computer program considering the interference effect was designed to obtain the predicted contours of the Zeeman structures of the lines. By variation of free parameters describing the line shapes and the electric-quadrupole admixtures, the calculated profiles were fitted to the recorded spectra. The *E*2 admixtures found are $(7.84 \pm 0.14)\%$, $(17.5 \pm 0.4)\%$, and $(0.70 \pm 0.11)\%$ for the 461.5, 647.6, and 875.5 nm lines, respectively. Our results are compared with recent theories and other experiments.

I. INTRODUCTION

The $6s^2 6p^3$ ground configuration of bismuth gives rise to five levels $^4S_{3/2}$, $^2P_{3/2,1/2}$, and $^2D_{5/2,3/2}$ (see Fig. 1). Since electric-dipole (*E*1) transitions between states of the same parity are forbidden, all the levels of the $6s^2 6p^3$ configuration are metastable. Weak magnetic-dipole (*M*1), electric-quadrupole (*E*2), and transitions allowed for both *M*1 and *E*2 types of radiation are permitted in second-order radiation theory.

When various components (corresponding to different M, M') of the atomic line of mixed $M1+E2$ character are separated as to wavelengths, an interference effect between different multipole radiations can be observed. In the theory, the intensity of Zeeman components $\Delta M = \pm 1$ is not a simple sum of intensities of the pure *E*2 and pure *M*1 radiation, but includes a cross term caused by the interference. The interference term can be positive or negative; it has different values for different components and changes with the direction of observation. The term reverses its sign when the observation is changed from parallel to perpendicular to the field.

This interference in the Zeeman effect was observed for the first time by Jenkins and Mrozowski [1]. The *M*1-*E*2 interference does not change the state of polarization of the emitted radiation, but in emission spectra, the effect produces a difference between the intensities of $\Delta M = \pm 1$ Zeeman patterns observed in the longitudinal and transverse directions. This phenomenon was used in a series of experiments for precise determination of the electric-quadrupole admixture in the forbidden lines. At the beginning of these studies, using photographic photometry, the intensities of separated groups of Zeeman patterns taken from the spectra obtained in longitudinal and transverse directions of observations (for σ and π polarizations) were compared with calculations for varying *E*2 admixture. The magnetic field and Fabry-Pérot spacers were selected in such a way that no overlap of different groups of Zeeman components was present [2–4]. Later, the photographic photometry was replaced by a simple visual comparison, to find the best match between the experimental microphotometer trace and a series of calculated profiles for varying *E*2 admixtures [5–7].

The *M*1-*E*2 interference in Bi I lines has been observed also in absorption by means of the Faraday effect [8–10]. These measurements were connected with atomic parity nonconservation experiments [11].

The *E*2 admixture measurement in forbidden lines is a very sensitive test for the theory, and because of the large discrepancy between experimental data [5,6] and theoretical predictions [12] we reexamined three mixed multipole lines of Bi I shown in Fig. 1.

II. EXPERIMENT

A standard experimental arrangement for observation of the Zeeman effect of forbidden lines was used. An electrodeless discharge tube powered by a rf generator (55 MHz) was the source of forbidden lines. The high-resolution spectral apparatus consisted of a silver-coated Fabry-Pérot étalon and Carl Zeiss Jena PGS-2 grating spectrograph (651.5 grooves/mm, resolution 0.8 nm/mm in the first order) combined with a charge-coupled device (CCD) detector (Hamamatsu model S7032-0906 with head device model C7042).

A Glan prism was used to separate the σ and π components. Observations were performed only for perpendicular view and π polarization.
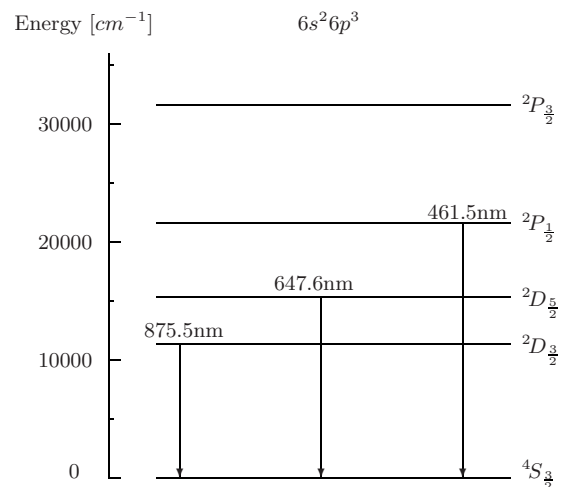

FIG. 1. Energy levels of the $6s^2 6p^3$ ground configuration of Bi I, with the observed mixed $M1+E2$ transitions.

*fizjk@univ.gda.pl

The light source was placed in a gap of a magnet producing fields up to 2 kG. The magnetic field was measured with an accuracy of 2% by the use of a gaussmeter (Applied Magnetics Laboratory model GM1A). Using the strong 605.9 nm $(6p8p\ ^3P_0 \rightarrow 6p7s\ ^3P_1)$ line of Pb I, we have calibrated the gaussmeter output to an absolut precision of 1%. In the calibration procedure we used the following set of data: $A(6p7s\ ^3P_1) = 293.60(5)$ mK [13], $g_J(6p7s\ ^3P_1) = 1.349$ [14].

III. THEORY

The probability of a mixed $M1 + E2$ transition between Zeeman states $|\gamma, J', I, F', M_F'\rangle$ and $|\gamma, J, I, F, M_F\rangle$ can be expressed as

$$
\begin{aligned}
a^{\text{total}}_{M_F', M_F} = \frac{1}{16\pi} \Bigg(& A^{M1}_{J'J} \sum_{q=-1}^{1} |b^{(0)}_{1q}(\theta)|^2 |\mathcal{S}^{(1)}_{qM_F'M_F}|^2 \\
& + A^{E2}_{J'J} \sum_{q=-2}^{2} |b^{(1)}_{2q}(\theta)|^2 |\mathcal{S}^{(2)}_{qM_F'M_F}|^2 \\
& \pm 2\sqrt{A^{M1}_{J'J} A^{E2}_{J'J}} \sum_{q=-1}^{1} [b^{*(0)}_{1q}(\theta) b^{(1)}_{2q}(\theta)] \mathcal{S}^{(1)}_{qM_F'M_F} \mathcal{S}^{(2)}_{qM_F'M_F} \Bigg)
\end{aligned}
\tag{1}
$$

(see [2,15–17]), where $\mathcal{S}^{(k)}_{qM_F'M_F}$ denotes

$$
\mathcal{S}^{(k)}_{qM_F'M_F} = \sum_{F', F} C^{*\gamma'}_{M_F'F'} \mathcal{S}^{(k)}_{qF'F} C^{\gamma}_{M_F F},
\tag{2}
$$

and

$$
\begin{aligned}
\mathcal{S}^{(k)}_{qF'F} = (-1)^{F' - M_F' + J' + I + F + k} \sqrt{(2F'+1)(2F+1)}\, \delta_{q, M_F' - M_F} \\
\times \begin{pmatrix} F' & k & F \\ -M_F' & q & M_F \end{pmatrix} \begin{Bmatrix} J' & F' & I \\ F & J & k \end{Bmatrix}.
\end{aligned}
\tag{3}
$$

The $C^{\gamma}_{M_F F}$ coefficients can be obtained by diagonalization of the Hamiltonian matrix consisting of two contributions: the hyperfine interaction of the nucleus with the electron shell and the energy of the atom in an external magnetic field [17].

In Eq. (1) the products $|b^{(0)}_{1q}(\theta)|^2$, $|b^{(1)}_{2q}(\theta)|^2$, and $[b^{*(0)}_{1q} \times (\theta) b^{(1)}_{2q}(\theta)]$, which connect the states of polarization of the emitted light with the direction of observation, can be written as

$$
|b^{(0)}_{10}|^2 = 6(|\varepsilon_2|^2)(1 - x^2),
\tag{4}
$$

$$
|b^{(0)}_{1\pm 1}|^2 = 3[|\varepsilon_1|^2 + |\varepsilon_2|^2 x^2 \pm i(\varepsilon_1^* \varepsilon_2 - \varepsilon_2^* \varepsilon_1)x],
\tag{5}
$$

$$
|b^{(1)}_{20}|^2 = 30(|\varepsilon_1|^2)(1 - x^2)x^2,
\tag{6}
$$

$$
\begin{aligned}
|b^{(1)}_{2\pm 1}|^2 = 5[|\varepsilon_1|^2 (2x^2 - 1)^2 + |\varepsilon_2|^2 x^2 \pm i(\varepsilon_1^* \varepsilon_2 - \varepsilon_2^* \varepsilon_1) \\
\times (2x^2 - 1)x],
\end{aligned}
\tag{7}
$$

$$
|b^{(1)}_{2\pm 2}|^2 = 5(1 - x^2)[|\varepsilon_1|^2 x^2 + |\varepsilon_2|^2 \pm i(\varepsilon_1^* \varepsilon_2 - \varepsilon_2^* \varepsilon_1)x],
\tag{8}
$$

$$
\begin{aligned}
b^{*(0)}_{1\pm 1} b^{(1)}_{2\pm 1} = \mp \sqrt{15}\{|\varepsilon_1|^2 (2x^2 - 1) + |\varepsilon_2|^2 x^2 \pm ix[\varepsilon_1^* \varepsilon_2 \\
- \varepsilon_2^* \varepsilon_1 (2x^2 - 1)]\},
\end{aligned}
\tag{9}
$$

where $x = \cos\theta$ ($x = 0$ for transverse and $x = 1$ for longitudinal directions of observation, respectively).

In deriving Eqs. (4)–(9) we used the coordinate system with the $\hat{z}$ axis directed along the magnetic field and the unit vectors of photon polarization $\vec{e}$ and propagation $\vec{n}$ determined by

$$
\vec{n} = \hat{y} \sin\theta + \hat{z} \cos\theta,
\tag{10}
$$

$$
\vec{e} = \varepsilon_2 \hat{x} + \varepsilon_1 (\hat{z} \sin\theta - \hat{y} \cos\theta),
\tag{11}
$$

where θ is the angle between the direction of the magnetic field and the direction of observation, and the parameters ε_1 and ε_2 are introduced in order to distinguish the contributions due to the two mutually orthogonal directions of polarization. For perpendicular observation and π polarization ($\Delta M = \pm 1$), we have $|b^{(0)}_{1,\pm 1}|^2 = 3$, $|b^{(1)}_{2,\pm 1}|^2 = 5$, and $(b^{*(0)}_{1,\pm 1} b^{(1)}_{2,\pm 1}) = \pm \sqrt{15}$.

Expression (1) shows that different magnetic and electric multipoles interfere. Therefore the transition probability for mixed transitions is not a simple sum of independent terms describing well-known pure multipole radiation of electric and magnetic types:

$$
A^{M1}_{J'J} = \frac{4}{3\hbar(4\pi\varepsilon_0 c^2)} \left(\frac{\omega}{c}\right)^3 |\langle \gamma' J' \| \hat{\mu}_1 \| \gamma J \rangle|^2,
\tag{12}
$$

$$
A^{E2}_{J'J} = \frac{1}{15\hbar(4\pi\varepsilon_0)} \left(\frac{\omega}{c}\right)^5 |\langle \gamma' J' \| \hat{Q}_2 \| \gamma J \rangle|^2.
\tag{13}
$$

However, the cross term vanishes after integration over photon polarizations and directions of observation. Then the interference can be observed only when various components of atomic line (corresponding to different M', M) are separated with respect to wavelength by means of the magnetic field.

Let us define the electric-quadrupole admixture in a mixed transition by

$$
D = \frac{A^{E2}_{J'J}}{A^{M1}_{J'J} + A^{E2}_{J'J}}.
\tag{14}
$$

Next, as a final step one may express the relative transition probability $a^{\text{rel}}_{M_F', M_F} = a^{\text{total}}_{M_F', M_F} / (A^{M1}_{J'J} + A^{E2}_{J'J})$ according to

$$
\begin{aligned}
a^{\text{rel}}_{M_F', M_F} = \frac{1}{16\pi} \{ & (1 - D)|b^{(0)}_{1q}(\theta)|^2 |\mathcal{S}^{(1)}_{M_F'M_F}|^2 \\
& + D|b^{(1)}_{2q}(\theta)|^2 |\mathcal{S}^{(2)}_{M_F'M_F}|^2 \\
& \pm 2\sqrt{D(1-D)} [b^{*(0)}_{1q}(\theta) b^{(1)}_{2q}(\theta)] \mathcal{S}^{(1)}_{M_F'M_F} \mathcal{S}^{(2)}_{M_F'M_F} \},
\end{aligned}
\tag{15}
$$

where $q = M_F' - M_F$.

The relative intensities of Zeeman patterns observed in the experiment are directly proportional to the relative transition probabilities $a^{\text{rel}}_{M_F', M_F}$.

The sign of the interference term in (1) can be predicted if the wave functions of the electronic states involved in the transition are known. It is determined by the sign of the product of the two reduced matrix elements $\langle \gamma' J' \| \hat{\mu}_1 \| \gamma J \rangle$ and $\langle \gamma' J' \| \hat{Q}_2 \| \gamma J \rangle$.

The phase (sign) of the interference term in (15) determines which of the calculated profiles corresponds to the π view and which to the L view. Our computer simulations show that the sign is negative for the Zeeman components of the 875.5 nm line and positive for the components of the 647.6 and 461.5 nm lines, in agreement with the signs of matrix elements calculated in [18]. This observation is in opposition to the phase rule expressed in [6]: for transitions between levels with hyperfine splitting constants A of the same signs the phase factor is positive, and for transitions between levels with A of opposite signs the phase factor is negative.

IV. COMPUTER SIMULATIONS

A direct observation of separate hfs Zeeman components is practically unachievable for conditions under which the hyperfine splitting is barely resolved. The number of Zeeman components runs into hundreds and interferes with hyperfine structure. What can be observed is an envelope of partially overlapping lines.

We assumed that the observed contour is described by the following intensity distribution function:

$$I(\nu) = I_0(\nu) + \sum_i \frac{I_i}{1 + \alpha_1^2(\nu - \tilde{\nu}_i)^2 + \alpha_2^4(\nu - \tilde{\nu}_i)^4}, \quad (16)$$

where $I_0(\nu)$ describes the background noise, I_i is the intensity of the ith Zeeman component directly proportional to the transition probability (15), $\tilde{\nu}_i = \nu_i + \nu_0$ is the position of the component on the frequency axis (ν_0 shifts the whole contour either left or right), and the parameters α_1 and α_2 describe the shape of the line. The function (16) is a convolution of Cauchy, Gauss, and approximate Airy functions [19,20]. The Cauchy and Gauss functions describe the radiative and Doppler broadenings of the atomic line, whereas the Airy profile is connected with the instrumental broadening.

In the computer simulations the least-square-fitting procedure was used. The simulated structure was fitted to the experimental curve recorded in the digital form. In our computations we used the set of data for hfs constants and experimental g_J factors presented in Table I.

The actual Fabry-Pérot pattern has a variable dispersion, especially near the center of the fringe system, but the simulated structure is calculated with a linear dispersion. In order to avoid this difficulty the experimental profile was linearized. Care was taken to keep the area under the interferometric curve constant. After linearization the profile was normalized. Then, by variation of the D value and line shape parameters α_1 and α_2, the simulated contour was fitted to the experimental data.

TABLE I. Values of the hyperfine structure constants A and B (in mK) and Landé g_J factors used in our computations.

	A	B	g_J
$^2P_{1/2}$	376[a]	0	0.6654(2)[b]
$^2D_{5/2}$	83.56(3)[c]	1.3(6)[c]	1.20[e]
$^2D_{3/2}$	−40.92(4)[d]	−20.58(33)[d]	1.225[e]
$^4S_{3/2}$	−14.90803(3)[b]	−10.17582(7)[b]	1.6433(2)[f]

[a]Reference [21].
[b]Reference [22].
[c]Reference [23].
[d]Reference [24].
[e]Reference [14].
[f]Reference [25].

V. RESULTS

A. The 461.5 nm line

The 461.5 nm line is the strongest of the forbidden lines of Bi I. The observations of the Zeeman effect were performed at four field values: 0.98, 1.23, 1.48, and 1.72 kG for the transverse direction of observation and π polarization. We used a 4 mm Fabry-Pérot spacer. Figure 2(a) shows the recorded Zeeman structure of the line at 1.48 kG field. The observed line contours were analyzed using the least-square-fitting procedure described in Sec. IV. Black dots represent the experimental results and the continuous line is the computer best fit described by formula (16). The "error" curve at the bottom of the picture presents the differences between the calculated and experimental contours. Figure 3(a) presents the computer simulations of Zeeman patterns for varying values of the electric-quadrupole admixture D. It shows the sensitivity of the shape of the generated structure to the D parameter changes.

We analyzed five interferometric orders for each value of the magnetic field. In order to generate a predicted pattern comparable with the recorded trace a simulation of overlapping of Fabry-Pérot orders had to be added to the computer's procedure.

All the results for D grouped into four runs are summarized in Table II. As an example Fig. 4(a) shows that a histogram of 99 measurements for set III (1.48 kG) is well fitted by a Gaussian curve.

The α_1 parameter values obtained from the fitting procedure varied from 0.07 to 0.09 cm^{-1}, and the values of α_2 varied in the range 0.1–0.3 cm^{-1}.

The weighted mean value from all our experimental results for different magnetic fields was determined to be $D = (7.84 \pm 0.05)\%$. Because the spread of the results for D is large, the χ^2 test gives a value 8, which is much higher than 1; the uncertainty should be multiplied by $\sqrt{\chi^2}$. Then the final result is $D = (7.84 \pm 0.14)\%$.

The final experimental value agrees with, but is somewhat lower than, our previous percentage admixture measurement [26] of $(7.7 \pm 0.4)\%$. In [26], the D value was obtained by simple hfs observation combined with the computer simulation technique. The Zeeman profile is much more sensitive to the $E2$ admixture changes [see Fig. 3(a)] than the hfs profile
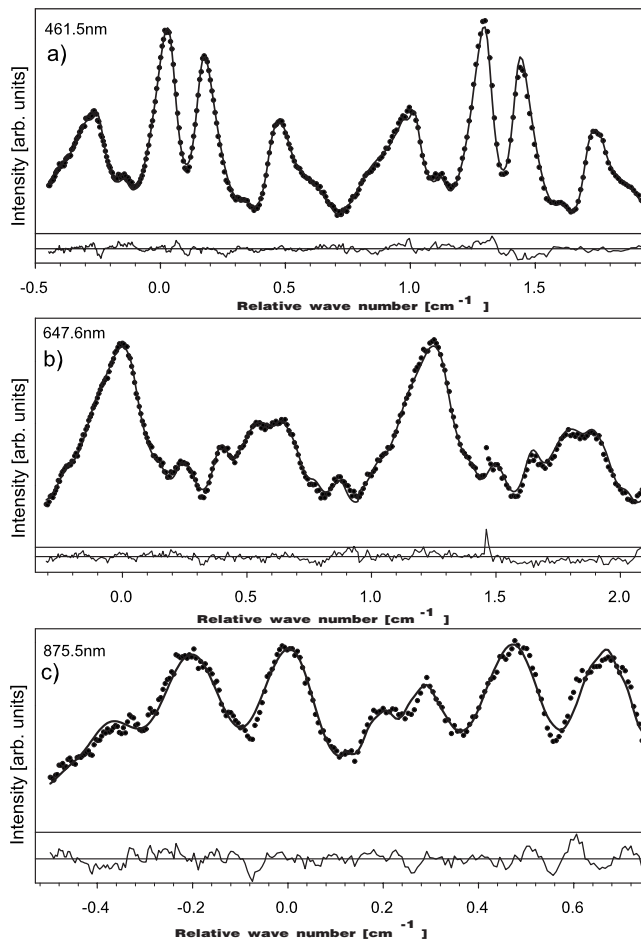
FIG. 2. Recorded Zeeman patterns: π views at 1.48 kG magnetic field for (a) 461.5 nm line with 4 mm spacer, (b) 647.6 nm line with 4 mm spacer, and (c) 875.5 nm line with 8 mm spacer. At the bottom of each figure is presented the residual curve describing deviations between calculated and observed profiles.

of the line [see Fig. 2(b) from [26]]. The present result, obtained by observation of the $M1$-$E2$ interference effect, is substantially more accurate.

B. The 647.6 nm line

The observations of the Zeeman effect were performed at four field values: 0.98, 1.23, 1.48, and 1.72 kG. We used 4

TABLE II. Observed ratio $D=A^{E2}/(A^{M1}+A^{E2})$ (in %) of the 461.5 nm line for four field values.

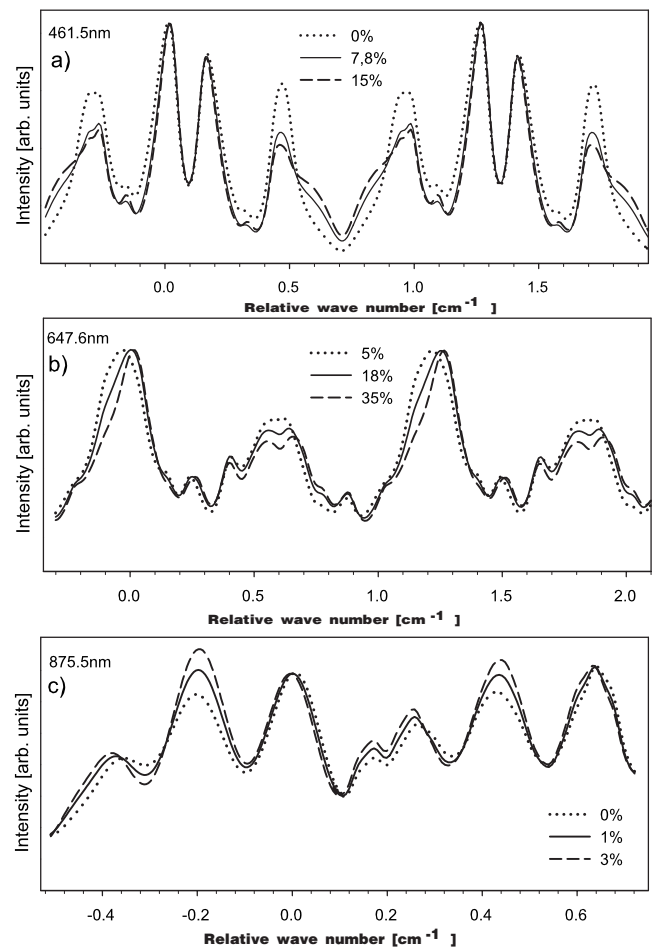| Magnetic field (kG)	$\langle D \rangle$	N [a]
0.98	8.02 ± 0.07	224
1.23	7.84 ± 0.12	72
1.48	7.83 ± 0.09	99
1.72	7.38 ± 0.11	40
$\langle D \rangle_W$	7.84 ± 0.14	

[a]N is the number of measurements.

FIG. 3. Computer-generated contours of Bi I lines at 1.48 kG magnetic field for different values of the $E2$ percentage admixture D for (a) 461.5 nm line ($D=0\%$, 7.8%, and 15%), (b) 647.6 nm line ($D=5\%$, 18%, and 35%), and (c) 875.5 nm line ($D=0\%$, 1%, and 3%). All contours are normalized to the intensities of the highest-peak maxima.

mm and 8 mm Fabry-Pérot spacers. Figure 2(b) shows the recorded Zeeman structure of the line with 4 mm spacer at 1.48 kG field.

All the obtained results for D varied in the range 16.00–18.50% (see Table III). All the results for D grouped into six

TABLE III. Observed ratio $D=A^{E2}/(A^{M1}+A^{E2})$ (in %) of the 647.6 nm line for four field values.

Magnetic field (kG)	$\langle D \rangle$	N
0.98	18.39 ± 0.19	121
	16.70 ± 0.31 [a]	60
1.23	16.00 ± 0.22	54
1.48	17.00 ± 0.19	62
	18.50 ± 0.27 [a]	50
1.72	17.90 ± 0.16	30
$\langle D \rangle_W$	17.5 ± 0.4	

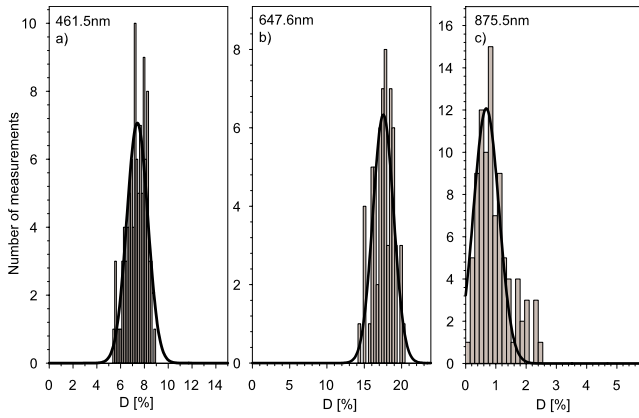[a]Results obtained with 8 mm spacer.

FIG. 4. (Color online) Histograms for distributions of the experimental data at 1.48 kG magnetic field for (a) 461.5 nm line, for a total of 99 individual measurements, (b) 647.6 nm line, for a total of 62 individual measurements, and (c) 875.5 nm line, for a total of 91 individual measurements.

runs are also summarized in Table III. Figure 4(b) shows a histogram of 62 measurements for set IV (1.48 kG). The α_1 parameter values obtained from the fitting procedure varied from 0.08 to 0.10 cm^{-1}, and the values of α_2 varied in the range 0.11–0.70 cm^{-1}.

The weighted mean value from all our experimental results for different magnetic fields was determined to be $D = (17.50 \pm 0.09)\%$. Because the spread of the results for D is large ($\chi^2 = 20$), the uncertainty should be multiplied by $\sqrt{\chi^2}$. Then the final result is $D = (17.5 \pm 0.4)\%$.

C. The 875.5 nm line

The observations of the Zeeman effect were performed at four field values: 0.98, 1.23, 1.48, and 1.74 kG. In this measurement care has been taken to avoid detection of parasitic blackbody radiation from the oven ensemble. However, a detectable contribution to the dark current was present in the recorded spectra. This problem was reduced by performing each run of intensity measurements preceded by the noise observation. In this measurement the radiation intensity from both sides of the atomic line signal was recorded. Then the average dark current was subtracted from the recorded spectra. We used 8 mm Fabry-Pérot spacer. With this spacer the whole hfs barely fitted into one order without overlap. As an

TABLE IV. Observed ratio $D = A^{E2}/(A^{M1} + A^{E2})$ (in %) of the 875.5 nm line for four field values.

Magnetic field (kG)	$\langle D \rangle$	N
0.98	0.81 ± 0.12	106
1.23	1.07 ± 0.06	87
1.48	0.57 ± 0.05	91
1.74	0.65 ± 0.03	118
$\langle D \rangle_W$	0.70 ± 0.11	

TABLE V. Comparison between experimental and theoretical results for $E2$ contribution in mixed $M1 + E2$ transitions in Bi I (in %).

Transition	Experiment	Theory
$(^2P_{1/2} \rightarrow {}^4S_{3/2})$	20[a]	10.1[b]
(461.5 nm)	7.3 ± 0.9 [c]	7.3[d]
	7.7 ± 0.4 [e]	23[f]
	$8-9$ [g]	
	10 ± 0.8 [h]	
	6.5 ± 0.5 [i]	
	7.4 ± 0.4 [j]	
	7.84 ± 0.14 [k]	
$(^2D_{5/2} \rightarrow {}^4S_{3/2})$	15 ± 5 [l]	20[b]
(647.6 nm)	17.6 ± 1.2 [c]	17[d]
	18 ± 4.5 [m]	34.5[f]
	16 ± 1 [i]	
	17.8 ± 1.0 [n]	
	19.5 ± 0.5 [o]	
	19.2 ± 1.5 [p]	
	17.5 ± 0.4 [k]	
$(^2D_{3/2} \rightarrow {}^4S_{3/2})$	2.25 ± 0.5 [q]	0.67[b]
(875.5 nm)	1 ± 1 [n]	0.5[d]
	0.82 ± 0.11 [r]	1.26[f]
	0.70 ± 0.11 [k]	

[a]Reference [29].
[b]Single-configuration approximation, Ref. [27].
[c]Reference [30].
[d]Semiempirical, Ref. [34].
[e]Reference [26].
[f]Multiconfiguration HFR, Ref. [12].
[g]Reference [31].
[h]Reference [2].
[i]Reference [5].
[j]Reference [17].
[k]Present work.
[l]Reference [32].
[m]Reference [3].
[n]Reference [8].
[o]Reference [33].
[p]Reference [23].
[q]Reference [6].
[r]Reference [24].

example, Fig. 2(c) shows the recorded Zeeman structure of the line at 1.48 kG field. We analyzed five interferometric orders for each value of the magnetic field.

All the obtained results for D varied in the range 0.57–1.07% for magnetic fields 1.48 and 1.23 kG, respectively (see Table IV). The α_1 parameter values obtained from the fitting procedure varied from 0.09 to 0.12 cm^{-1}, and the values of α_2 varied in the range 0.11–0.70 cm^{-1}.

The final value from all our experimental results for different magnetic fields was determined to be $D = (0.70 \pm 0.11)\%$ (the measurement uncertainty was multiplied by $\sqrt{\chi^2}$).

VI. COMPARISON BETWEEN EXPERIMENTAL AND THEORETICAL RESULTS

The calculated multipole transition rates are particularly sensitive to even small modifications to the wave functions and a careful choice of the theoretical method is required—very often the theoretical predictions disagree with experiment.

For the Bi I spectrum, neither LS nor jj coupling is adequate. The intermediate coupling in the fine structure of the $6s^26p^3$ configuration in the single-configuration approximation has been studied by several authors [22,27,28]. A complete list of $M1$ and $E2$ transition probabilities for the $6s^26p^3$ ground configuration of Bi I has been published in [27]. The most extensive multiconfiguration calculations of multipole transition rates have been performed by Biémont and Quinet [12], by the use of the relativistic Hartree-Fock (HFR) method.

In Table V our result was compared with theory and experimental results of other authors. From the table it follows that our result is consistent with recent experimental data. These results have been obtained by using different spectroscopic methods. The $E2$ admixtures in papers [26,29,30,32] have been obtained by simple hfs measurements, the results presented in papers [5,6,17] originated from observation of the Zeeman effect, and those presented in papers [8,23,24,33] are the results of Faraday rotation measurements. The quantity directly measured in the Faraday effect is the ratio χ of amplitudes for the $M1$ and $E2$ transitions, which is related to the electric-quadrupole admixture D by $D=3\chi^2/(3\chi^2+5)$.

The measured $E2$ admixtures can be compared with theoretical predictions. As follows from the table, a good agreement can be achieved in single-configuration calculations presented in [27] and [34]; in paper [34] the intermediate coupling wave functions from [22] and the experimental value of the radial integral s_q of r^2 between single-electron states, $s_q=8.7ea_0^2$, from [8] were used. However, there is a large discrepancy between values obtained by us and the HFR results. The HFR method allows consideration of a large number of interacting configurations (14 configurations), but only approximately accounts for the relativistic effects, which are crucial for heavy elements. Nevertheless, the HFR energies obtained in [12] appear to be in very good agreement with experimental data.

A comparison between the single-configuration approximation and the HFR method shows that the situation in calculations of transition probabilities is very complex. In the case of the ground configuration of Bi I, the effect of configuration mixing is very weak, and limited inclusion into calculations of admixtures of several selected configurations does not necessarily give reliable results for transition rates, even if the calculated energy levels agree very well with observation.

VII. CONCLUSION

We conclude that our measurement yields very accurate electric-quadrupole admixtures in multipole lines of Bi I. Our result is consistent with recent experimental data, but in strong disagreement with results of multiconfiguration HFR calculations.

[1] F. A. Jenkins and S. Mrozowski, Phys. Rev. **60**, 225 (1941).

[2] S. T. Dembiński, J. Heldt, and L. Wolniewicz, J. Opt. Soc. Am. **62**, 555 (1972).

[3] L. Augustyniak, J. Heldt, and J. Bronowski, Phys. Scr. **12**, 157 (1975).

[4] J. Czub, J. Heldt, and A. Kowalczyk, Acta Phys. Pol. A **44**, 609 (1973).

[5] J. Czerwińska, J. Opt. Soc. Am. B **4**, 1349 (1987).

[6] J. Czerwińska and S. Mrozowski, J. Opt. Soc. Am. B **8**, 940 (1991).

[7] S. Mrozowski, J. Czerwińska, and R. Drozdowski, J. Opt. Soc. Am. B **10**, 607 (1993).

[8] G. J. Roberts, P. E. G. Baird, M. W. S. M. Brimicombe, P. G. H. Sanders, D. R. Selby, and D. N. Stacey, J. Phys. B **13**, 1389 (1980).

[9] D. C. Soreide and E. N. Fortson, Bull. Am. Phys. Soc. **20** (2), 491 (1975).

[10] D. C. Soreide, D. E. Roberts, E. G. Lindahl, L. L. Lewis, G. R. Apperson, and E. N. Fortson, Phys. Rev. Lett. **36**, 352 (1976).

[11] E. N. Fortson and L. L. Lewis, Phys. Rep. **113**, 289 (1984).

[12] E. Biémont and P. Quinet, Phys. Scr. **54**, 36 (1996).

[13] S. Bouazza, D. S. Gough, P. Hannaford, R. M. Lowe, and M. Wilson, Phys. Rev. A **63**, 012516 (2000).

[14] Ch. Moore, *Atomic Energy Levels*, Natl. Bur. Stand. (U.S.) Circ. No. 467 (U.S. GPO, Washington, D.C., 1958), Vol. III.

[15] E. Gerjuoy, Phys. Rev. **60**, 233 (1941).

[16] J. Heldt and J. Kwela, Acta Phys. Pol. A **66**, 461 (1984).

[17] S. Werbowy, J. Kwela, R. Drozdowski, and J. Heldt, Eur. Phys. J. D **39**, 5 (2006).

[18] G. H. Shortly, L. H. Aller, J. G. Baker, and D. H. Menzel, Astrophys. J. **93**, 178 (1941).

[19] H. Hühnermann, Ph.D. thesis, Philips-Universitat Marburg/Lahn, 1967 (unpublished).

[20] G. Müller, Dissertation, Technische Universität Berlin, 1974 (unpublished).

[21] L. O. Dickie and F. M. Kelly, Can. J. Phys. **45**, 2249 (1967).

[22] D. A. Landman and A. Lurio, Phys. Rev. A **1**, 1330 (1970).

[23] D. M. Lucas, R. B. Warrington, C. D. Thompson, and D. N. Stacey, J. Phys. B **27**, 5497 (1994).

[24] K. M. J. Tregidgo, P. E. G. Baird, M. J. D. Macpherson, C. W. P. Palmer, P. G. H. Sandars, D. N. Stacey, and R. C. Thompson, J. Phys. B **19**, 1143 (1986).

[25] R. S. Title and K. F. Smith, Philos. Mag. **5**, 1281 (1960).

[26] S. Werbowy and J. Kwela, Eur. Phys. J. Spec. Top. **144**, 179 (2007).

[27] R. H. Garstang, J. Res. Natl. Bur. Stand., Sect. A **68**, 61 (1964).

[28] E. U. Condon and G. H. Shortley, *The Theory of Atomic Spec-*

tra (Cambridge University Press, Cambridge, U.K., 1963).

[29] J. Heldt, J. Opt. Soc. Am. **58**, 1516 (1968).

[30] T. J. Wasowicz, Phys. Scr. **76**, 294 (2007).

[31] J. Heldt and S. Mrozowski, J. Opt. Soc. Am. **60**, 467 (1970).

[32] J. Heldt, T. Gil, S. Zachara, and M. Hults, J. Opt. Soc. Am. B **1**, 48 (1984).

[33] Yu. V. Bogdanov, S. I. Kanorskii, I. I. Sobel'man, V. N. So-rokin, I. I. Struk, and E. A. Yukov, Opt. Specktrosk. **61**, 281 (1986) [Opt. Spectrosc. **61** 446 (1986)].

[34] P. Horodecki, J. Kwela, and J. E. Sienkiewicz, Eur. Phys. J. D **6**, 435 (1999).